[17] Rothe, D. E., "Electron-Beam Studies of Low Reynolds Number Flows inside a DeLaval Nozzle," AIAA Paper 70-810, Los Angeles, 1970.

[18] Lefkowitz, B. and Knuth, E. L., "A Study of Rotational Relaxation in a Low-Density Hypersonic Free Jet by Means of Impact-Pressure Measurements," *Proceedings of the Sixth International Symposium on Rarefied Gas Dynamics*, Vol. II, 1969, M.I.T., Cambridge, Mass., pp. 1421–1438.

[19] Love, E. S. et al., "Experimental and Theoretical Studies of Axisymmetric Free Jets," TR R-6, 1959, NASA.

MAY 1971 AIAA JOURNAL VOL. 9, NO. 5

Some Numerical Results on Viscous Low-Density Nozzle Flows in the Slender-Channel Approximation

WILLIAM J. RAE*
Cornell Aeronautical Laboratory, Buffalo, N.Y.

Calculated results are presented for converging-diverging nozzle flows in which viscous effects are important across the entire nozzle cross section. The slender-channel equations are used, with slip boundary conditions at the walls. The solution is started upstream of the throat, using asymptotic results for slow viscous flow in a converging cone. An implicit finite-difference scheme is then used to calculate the pressure, and profiles of velocity and enthalpy at successive stations along the channel. The cases chosen for presentation show the effects of varying the nozzle geometry, the Reynolds number, and the thermal condition of the nozzle wall. The results suggest that specific impulse is improved by a throat whose longitudinal radius of curvature is small, and that exit area ratios as low as ten can be used without serious loss of performance. It is shown that, at sufficiently low Reynolds numbers and low exit-cone angles, there is no solution of the slender-channel equations in which the flow can expand to supersonic conditions. Instead, the boundary layer closes, and the solution resembles a viscous subsonic pipe flow. The implications of this finding on the upstream influence of the exit-plane conditions and on the limits of validity of the slender-channel equations are discussed.

Nomenclature

a = speed of sound
A = $\dot{m}/2\pi\rho_0(2H_0)^{1/2}r_*^2$
A/A_* = geometric area ratio
B = $\rho_0(2H_0)^{1/2}r_*/\mu_0$
D = ρ/ρ_0
F = thrust
$\bar{F}$ = $F/p_0\pi r_*^2$
h = static enthalpy
H = total enthalpy
$\dot{H}$ = $\sigma_w^2\int_0^1 \eta DU(\Theta + U^2)d\eta$; see Eq. (25)
k = thermal conductivity
$\dot{m}$ = mass flow rate
M = Mach number
$\mathfrak{M}$ = molecular weight
p = pressure
P = p/p_0
Pr = Prandtl number
Q = $(1/B)[\Theta^\omega(\partial/\partial\eta)(\Theta/Pr + U^2)]_{\eta=1}$ heat transfer from the wall to the gas corresponds to $Q > 0$
r,z = cylindrical coordinates
r_1 = longitudinal radius of curvature of the nozzle wall, at the throat
r_* = transverse radius of the nozzle throat
$\mathfrak{R}$ = universal gas constant
$R(z)$ = transverse radius of nozzle wall
R_1 = r_1/r_*
T = temperature
u,v = axial and radial velocity components
U,V = $u/(2H_0)^{1/2}$, $v/(2H_0)^{1/2}$
W = $V - U\eta d\sigma_w/dx$
x,σ = z/r_*, r/r_*
α_u,α_T = accommodation coefficients for velocity and temperature
γ = specific-heat ratio
δ_1 = displacement thickness
η = σ/σ_w
θ = wall angle
θ_1,θ_2 = entrance and exit cone angles, Sec. IV
Θ = h/H_0
μ = viscosity
ρ = density
σ = r/r_*
ω = exponent in viscosity, enthalpy relation
$(\ )_e$ = conditions at nozzle-exit plane
$(\ )_0$ = conditions in reservoir
$(\ )_W$ = conditions at the wall
$(\ )_\mathfrak{C}$ = conditions on the axis
$(\ )_*$ = conditions at the geometric throat

Presented as Paper 69-654 at the AIAA Fluid and Plasma Dynamics Conference, San Francisco, Calif., June 16–18, 1969; submitted March 13, 1970; revision received December 18, 1970. Research sponsored by NASA under Contract NASW-1668. Technical direction was provided by M. Curtis of the Goddard Space Flight Center and F. E. Compitello of NASA Headquarters; their advice and encouragement are gratefully acknowledged. The author is also grateful to his colleagues J. A. Lordi and P. V. Marrone for many discussions of this work, and to J. R. Moselle for his very capable handling of the computer programming.

* Principal Research Engineer, Aerodynamic Research Department. Member AIAA.

I. Introduction

THE rocket engines that are used for satellite attitude control are often required to produce a thrust less than one pound-force, extending in some instances to values as low as

10^{-6} lbf.[1] Such low values of the thrust dictate the use of low reservoir pressures and small nozzle scale; the result is that the flow takes place at very low Reynolds numbers, where viscous effects are felt all across the nozzle cross section. Thus, it is not possible to calculate the performance of these devices by the usual inviscid, one-dimensional flow approximation, with a small correction due to a thin boundary layer.

The studies described in this paper were undertaken with the objective of predicting nozzle flows in the Reynolds-number range appropriate to the operation of microthrust rockets. The results found also have application to the flowfields in low-density wind tunnels.

The approaches that have previously been applied to this problem can be grouped in three categories. In the first, applicable at the high-Reynolds-number limit, it is assumed that the flow has an inviscid core that can be treated as an isentropic, one-dimensional channel flow. The boundary layer that forms on the walls is treated in a variety of ways, (e.g., by integral methods or by local application of similarity solutions) and its growth rate is usually coupled to the rate of expansion of the inviscid core. In developing this approach, various authors have used a number of further approximations; important among these are the degree to which transverse curvature is accounted for, and the manner of specifying the initial state of the boundary layer. Representative examples of this approach can be found in Refs. 2–7.

The second category of solutions is that appropriate to the very low-Reynolds-number limit, where the methods of kinetic theory are used. In this limit, the basic statistical physics of the flow are extremely complex. Thus, while the problem can be formulated, it is very difficult to achieve a solution of what might be called the "direct" problem, i.e., the problem of finding the flowfield for given nozzle geometry and given reservoir conditions.

The third category of solutions, employed in the present study, is based on the "slender-channel" equations. In this approximation, first proposed by Williams,[8,9] the Navier-Stokes equations are simplified on the basis that the channel walls diverge very slowly. Slip boundary conditions have been used, since it has been found in many studies (see, e.g. Ref. 10) that these conditions, with the Navier-Stokes equations, lead to valid results well down into the transition-flow regime.

The slender-channel equations are formally identical with the boundary-layer equations, including the full effect of transverse curvature. They differ only in being written in cylindrical coordinates aligned with the nozzle axis, rather than in surface coordinates. In this approximation the pressure is constant across the channel, varying only with distance along the channel. Thus, except for the boundary conditions, the slender-channel equations are the same as those often used in studies of the laminar axisymmetric wake. Finite-difference solutions for the latter problem have been presented by several groups[11–14] and suggested that the same techniques could be adapted to the nozzle-flow case. A brief description of the numerical method used is given in Sec. III.

In contrast to the thin-boundary-layer case, it is not possible in the present problem to establish the initial conditions at the throat. Instead, it is necessary to start the solution farther upstream, at near-reservoir conditions. Asymptotic solutions for the flow in a converging cone were used for this purpose, and are presented in Sec. IV. The results of typical calculations are given in Sec. V, and some general observations regarding the significance of the results are made in Sec. VI.

II. Basic Equations

The starting point for the derivation of the slender-channel equations is the Navier-Stokes equations. Williams simplified these by assuming that the ratio of radial to axial velocity components, and the ratio of axial to radial gradients were each of the order of the slenderness ratio of the nozzle.

In this approximation, the leading terms are

$$(\partial/\partial z)(\rho u) + (\partial/\partial r)(\rho v) + \rho v/r = 0 \tag{1}$$

$$\rho u \partial u/\partial z + \rho v \partial u/\partial r = -dp/dz + (1/r)(\partial/\partial r)(\mu r \partial u/\partial r) \tag{2}$$

$$\partial p/\partial r = 0 \tag{3}$$

$$\rho u \frac{\partial h}{\partial z} + \rho v \frac{\partial h}{\partial r} - u \frac{dp}{dz} = \frac{1}{r} \frac{\partial}{\partial r} \left(\frac{r\mu}{Pr} \frac{\partial h}{\partial r} \right) + \mu \left(\frac{\partial u}{\partial r} \right)^2 \tag{4}$$

These equations are formally identical with the boundary-layer equations, including the radial dependences that account for transverse curvature.

The boundary conditions applied at the walls are those corresponding to first-order velocity slip and temperature jump. The first of these relates the velocity component along the wall to its gradient normal to the wall. When this component is expressed as a linear combination of u and v and is then simplified according to the slender-channel ordering, the result is

$$-u_W = [(2 - \alpha_u)/\alpha_u](\mu/p)[(\pi/2)\Re T/\mathfrak{M}]^{1/2} \cos\theta (\partial u/\partial r)_W \tag{5}$$

The corresponding condition for the temperature becomes

$$T - T_W = -\frac{2 - \alpha_T}{\alpha_T} \frac{2\gamma}{Pr(\gamma + 1)} \frac{\mu}{p} \left(\frac{\pi}{2} \frac{\Re T}{\mathfrak{M}} \right)^{1/2} \times \cos\theta \left(\frac{\partial T}{\partial r} \right)_W \tag{6}$$

In all of the results presented in this paper, the gas has been assumed to follow the perfect-gas law, with constant Prandtl number, constant specific-heat ratio, and with viscosity proportional to a power of the temperature:

$$p = [(\gamma - 1)/\gamma]\rho h; \quad Pr = \text{const}; \quad \mu/\mu_0 = (h/H_0)^\omega \tag{7}$$

Dimensionless Forms

The reference quantities are chosen to be the reservoir values, and the coordinates are made dimensionless by the nozzle throat radius:

$$x = z/r_*, \ \sigma = r/r_* \tag{8}$$

and the dependent variables are made dimensionless with respect to reservoir conditions:

$$\begin{aligned} U &= u/(2H_0)^{1/2}, \ V = v/(2H_0)^{1/2} \\ P &= p/p_0, \ D = \rho/\rho_0, \ \Theta = h/H_0 \end{aligned} \tag{9}$$

In addition, it is useful to normalize the radial coordinate by its wall value at each station

$$\eta = \sigma/\sigma_W(x) \tag{10}$$

In terms of these variables, the equations of motion become

Continuity:

$$P(\partial/\partial\eta)(\eta W/\Theta) + \sigma_W \eta (\partial/\partial x)(PU/\Theta) + 2\sigma_W' P\eta U/\Theta = 0 \tag{11}$$

Momentum:

$$\frac{P}{\Theta}\left(U \frac{\partial U}{\partial x} + \frac{W}{\sigma_W} \frac{\partial U}{\partial \eta} \right) = -\frac{\gamma - 1}{2\gamma} \frac{dP}{dx} + \frac{1}{B\eta\sigma_W^2} \frac{\partial}{\partial\eta} \left(\eta\Theta^\omega \frac{\partial U}{\partial\eta} \right) \tag{12}$$

Energy:

$$\frac{P}{\Theta}\left(U\frac{\partial\Theta}{\partial x}+\frac{W}{\sigma_W}\frac{\partial\Theta}{\partial\eta}\right)=\frac{\gamma-1}{\gamma}U\frac{dP}{dx}+\frac{1}{B\eta\sigma_W{}^2}\frac{\partial}{\partial\eta}\left(\frac{\eta}{Pr}\Theta^\omega\frac{\partial\Theta}{\partial\eta}\right)+\frac{2\Theta^\omega}{B\sigma_W{}^2}\left(\frac{\partial U}{\partial\eta}\right)^2 \quad (13)$$

In these equations, the density has been eliminated by use of the equation of state:

$$P=D\Theta \quad (14)$$

The transformed radial velocity W that appears in these equations is

$$W=V-U\eta d\sigma_W/dx \quad (15)$$

Note that W is zero both at the wall and on the axis.

The only parameter that appears in these equations [in addition to γ, Pr, ω, and $\sigma_W(x)$] is a Reynolds number based on reservoir conditions and the throat radius:

$$B=\rho_0(2H_0)^{1/2}r_*/\mu_0 \quad (16)$$

This parameter is convenient to use, since it involves only conditions that are known in advance and are accessible to the designer.

The boundary conditions in the (x,η) coordinate system are:

$$U)_{\eta\to1}=-\frac{2-\alpha_u}{\alpha_u}\left(\frac{\pi\gamma}{\gamma-1}\right)^{1/2}\frac{\cos\theta}{BP\sigma_W}(\Theta_{\eta\to1})^{\omega+1/2}\times\left(\frac{\partial U}{\partial\eta}\right)_{\eta\to1} \quad (17)$$

If the wall temperature is prescribed, the thermal boundary condition is

$$\Theta_{\eta\to1}-\Theta_W(x)=-\frac{2-\alpha_T}{\alpha_T}\frac{2\gamma}{Pr(\gamma+1)}\left(\frac{\pi\gamma}{\gamma-1}\right)^{1/2}\times\frac{\cos\theta}{BP\sigma_W}(\Theta_{\eta\to1})^{\omega+1/2}\left(\frac{\partial\Theta}{\partial\eta}\right)_{\eta\to1} \quad (18)$$

If the wall is taken to be adiabatic, this second boundary condition is replaced by [See Eq. (25)]:

$$(\partial/\partial\eta)(\Theta/Pr+U^2)_{\eta\to1}=0 \quad (19)$$

On the axis, symmetry requires that

$$\partial U/\partial\eta_{\eta=0}=\partial\Theta/\partial\eta_{\eta=0}=0$$

Conservation Relations

The relations that express the global conservation of mass, momentum, and energy can be written down either from a direct transformation of the integral forms of the conservation laws, or by manipulation of Eqs. (11–13). The continuity equation, when integrated from zero to η, becomes an expression for W:

$$\eta W/\sigma_W\Theta\int_0^\eta\frac{\eta U}{\Theta}d\eta+\frac{d}{dx}\ln\left[P\sigma_W{}^2\int_0^\eta\frac{U\eta d\eta}{\Theta}\right]=0 \quad (20)$$

In particular, if the upper limit is set equal to one, (where $W=0$) this becomes an expression for the total mass flow:

$$P\sigma_W{}^2\int_0^1\frac{U\eta d\eta}{\Theta}=A\equiv\dot m/2\pi\rho_0r_*{}^2(2H_0)^{1/2} \quad (21)$$

The parameter A is proportional to the discharge coefficient of the nozzle:

$$C_D=2A[(\gamma+1)/2]^{1/(\gamma-1)}[(\gamma+1)/(\gamma-1)]^{1/2} \quad (22)$$

Integration of the momentum equation leads to an expression for the variation of the thrust coefficient:

$$d\bar F/dx=P(d/dx)(\sigma_W{}^2)+[4\gamma/B(\gamma-1)][\Theta(1)]^\omega\partial U/\partial\eta_{\eta=1} \quad (23)$$

where

$$\bar F\equiv\frac{F}{p_0\pi r_*{}^2}=P\sigma_W{}^2\left\{1+\frac{4\gamma}{\gamma-1}\int_0^1\frac{U^2\eta}{\Theta}d\eta\right\} \quad (24)$$

Equation (23) states that the maximum thrust occurs at the point where the contribution from the pressure forces acting on the wall is balanced by the viscous shear stress at the wall, an observation that has been made by many authors (see, for example, Ref. 15).

If the momentum equation is multiplied by $2U$, integrated, and added to the integrated energy equation, the result is a statement that the flux of total enthalpy is changed only by heat transfer at the wall:

$$\frac{d}{dx}\left\{\sigma_W{}^2\int_0^1\eta DU(\Theta+U^2)d\eta\right\}=\frac{1}{B}\left[\Theta^\omega\frac{\partial}{\partial\eta}\left(\frac{\Theta}{Pr}+U^2\right)\right]_{\eta=1} \quad (25)$$

The adiabatic wall boundary condition, cited above as Eq. (19), is found by setting the right-hand side of this expression equal to zero.

Streamtube Relation

In the study of isentropic, one-dimensional channel flows, a very important equation is the one that relates the pressure gradient to the rate of change of cross-sectional area.[16] For the present problem, this expression can be generalized to include the effects of viscosity. The generalization to viscous, two-dimensional flows was given by Weinbaum and Garvine[17]; the further generalization to the case of axisymmetric flows is given below.†

The equation of state is first used to eliminate the density from the continuity equation; in the resulting expression, the momentum and energy equations are used to replace $\partial u/\partial z$ and $\partial h/\partial z$ in favor of dp/dz. The result is

$$\frac{\partial}{\partial r}\left(r\frac{v}{u}\right)=-\frac{r}{\gamma p}\frac{M^2-1}{M^2}\frac{dp}{dz}-\frac{1}{\gamma pM^2}\frac{\partial}{\partial r}\left(\mu r\frac{\partial u}{\partial r}\right)+\frac{\gamma-1}{\gamma up}\frac{\partial}{\partial r}\left(\frac{\mu r}{Pr}\frac{\partial h}{\partial r}\right)+\frac{\gamma-1}{\gamma}\frac{\mu r}{up}\left(\frac{\partial u}{\partial r}\right)^2 \quad (26)$$

The left-hand side of this expression is proportional to the radial gradient of the streamline direction, and hence to the axial rate of change of cross-sectional area of the streamtube. Thus, the first two terms in Eq. (26) are exactly the same as those familiar from the case of isentropic, one-dimensional channel flows. The additional terms represent the contributions to the area change that come from shear, net heat conduction to the streamtube, and heat generation within the streamtube due to the conversion of kinetic to thermal energy. These terms can be checked against the equivalent expressions derived from first principles by Shapiro.[19]

In terms of the dimensionless variables, the streamtube relation is

$$\frac{\partial}{\partial\eta}\left(\eta\frac{V}{U}\right)=\frac{1-M^2}{\gamma M^2P}\eta\sigma_W\frac{dP}{dx}-\frac{2}{(\gamma-1)B\sigma_WPM^2}\times\left\{\frac{\partial}{\partial\eta}\left(\eta\Theta^\omega\frac{\partial U}{\partial\eta}\right)-\frac{U}{\Theta}\left[\frac{\partial}{\partial\eta}\left(\frac{\eta\Theta^\omega}{Pr}\frac{\partial\Theta}{\partial\eta}\right)+2\eta\Theta^\omega\left(\frac{\partial U}{\partial\eta}\right)^2\right]\right\} \quad (27)$$

† The axisymmetric formulas have also been presented in a recent paper by Garvine and Weinbaum.[18]

If this expression is now integrated across the channel, it becomes a relation between the rate of change of the total channel cross-sectional area, and the integrated effects of pressure gradient, shear, heat conduction, and heat generation. It is useful to solve the resulting expression for the pressure gradient:

$$\frac{dP}{dx} = \left\{ \gamma P \sigma_W' + \frac{2\gamma}{(\gamma - 1)B\sigma_W} \times \right.$$
$$\left. \int_0^1 \frac{\partial}{\partial \eta}\left(\eta\Theta^\omega \frac{\partial U}{\partial \eta}\right) - \frac{U}{\Theta}\left[\frac{\partial}{\partial \eta}\left(\frac{\eta\Theta^\omega}{Pr}\frac{\partial \Theta}{\partial \eta}\right) + 2\eta\Theta^\omega\left(\frac{\partial U}{\partial \eta}\right)^2\right]}{M^2} \times$$
$$d\eta \right\} \div \left\{ \sigma_W \int_1^0 \frac{1 - M^2}{M^2}\, \eta d\eta \right\} \quad (28)$$

In the limit of infinite Reynolds numbers, this expression reduces to the familiar inviscid, one-dimensional channel-flow result. At large finite Reynolds numbers, the general character of the solutions for various mass flows is qualitatively the same as that of the inviscid limit, namely: at sufficiently low mass flows, the pressure decreases along the converging part of the channel, reaches a minimum at or slightly beyond the throat, and then rises. For somewhat higher mass flows, the denominator of Eq. (28) changes sign upstream of the throat. Thus the pressure gradient becomes infinite, indicating that the flow has choked. At some intermediate mass flow, it is possible to find a saddle point, where the numerator and denominator of Eq. (28) vanish simultaneously. This intermediate mass flow is the only one that allows an expansion to conditions that are "supersonic," in the sense that

$$\int_0^1 \frac{1 - M^2}{M^2}\, \eta d\eta < 0$$

Thus for high Reynolds numbers there is a critical mass flow, which allows a supersonic flow. Greater mass flows lead to choking, while lower ones yield a subsonic flow in which the pressure reaches a minimum near the throat and then rises. The results given in Sec. V illustrate these types of behavior.

However, the results also show that the saddle point moves farther downstream as the Reynolds number is lowered, and that at low enough Reynolds numbers it does not occur at all within the range of exit-area ratios normally of interest in rocket design. For these cases, there is no mass flow that leads to supersonic conditions in the average sense indicated above. There is a certain mass flow for which choking occurs at the exit plane. For higher mass flows, choking occurs within the nozzle; for lower mass flows, the pressure may either reach a minimum and then rise, or it may decrease monotonically to the exit plane if the pressure drop due to friction is great enough to overcome the effect of nozzle expansion.

It should be noted that in cases where the no-slip condition is applied to the velocity at the wall, the integrals in Eq. (28) diverge. In order to obtain a determinate result, some account must be taken of the fact that in Eq. (27) the pressure gradient and shear-stress terms, as well as the heat-conduction and heat-generation terms, cancel in pairs in a region near the wall. Thus the simplification employed by Lighthill[20] might be used, in which the integration is stopped short of the wall. In the present paper, all of the cases studied allow slip at the walls, and the integrals can be carried out to $\eta = 1$ without complications.

III. Numerical Methods

Previous Solutions

Most of the existing solutions of the slender-channel equations are those of the self-similar variety, done by Williams[8,9,21,22]‡ and by Adams.[23] These solutions have given important qualitative information about low-density nozzle flowfields. However, they are of limited value when applied to the direct problem, since the conditions for self-similarity require nozzles whose shape changes when the Reynolds number is changed.

In recent years, many nonsimilar boundary-layer problems have been treated successfully by numerical methods (see, for example, Refs. 24 and 25) and it appeared that these methods could readily be adapted to the present problem. Numerical solutions of the slender-channel equations have in fact been presented by Milligan[26] and by Myers[27]; only a few such results are available however, due primarily to limitations in computational facilities.

Difference Equations

The coordinates are expressed as

$$x = x_0 + (K - 1)\Delta x,\ \eta = (L - 1)\Delta\eta,\ L = 1,2,\ \ldots,\ L_{\max}$$

(For all the calculations reported here, $L_{\max}$ was taken as 101.) Values of the dependent variables at a grid point are represented by the notation

$$U(x,\eta) = U_K{}^L$$

Crank-Nicholson implicit differences were used to represent the momentum and energy equations. Full details of the difference equations used are given in Ref. 29. These equations are a set of simultaneous algebraic equations for the values of U and Θ at the grid points across the channel.

Once a set of initial profiles and a value of dP/dx are given, the solution of the finite-difference equations can be determined recursively, following the method outlined by Richtmeyer and Morton.[28]

Pressure-Gradient Determination

In advancing the solution from station K to $K + 1$, the pressure gradient (assumed constant across the step) must be chosen so as to satisfy the three global conservation relations given above, as well as the integrated streamtube-area relation. Since the two difference equations being used are local expressions for the conservation of momentum and energy, it might be expected that the best choice would be to use the value of dP/dx that satisfies either the total mass conservation or the integrated streamtube-area relation. The computer program uses both of these options; it has been found that solutions determined with either option also satisfy the total momentum and energy conservation. Furthermore, except in the near vicinity of the saddle point, solutions found with either option also satisfy the other option. Near the saddle point, it is more accurate to use the streamtube relation; in most of the solutions described here, the pressure gradient has been determined in such a way as to enforce mass conservation up to the saddle point, and such as to satisfy the streamtube relation downstream of the saddle point.

The specific procedure used in enforcing mass conservation is as follows: a value of dP/dx is chosen, and the difference equations are solved for the profiles of U and Θ at station $K + 1$. These profiles are then used in Eq. (21) to calculate the pressure at the end of the step:

$$P_{K+1} = \left(A/\sigma_W{}^2 \int_0^1 \frac{U\eta d\eta}{\Theta} \right)_{K+1} \quad (29)$$

This pressure is compared with the value that would be found by extrapolating from the beginning of the step, and an iteration on dP/dx is performed until these two pressures are

‡ The solutions of Refs. 21 and 22 are solutions of the full Navier-Stokes equations.

equal, i.e.,

$$P_K + (dP/dx)\Delta x = P_{K+1} \tag{30}$$

The same type of procedure is used in choosing dP/dx so as to satisfy the integrated streamtube-area relation: a value of dP/dx is chosen, the difference equations are solved for U and Θ at station $K + 1$, and these profiles are then used to calculate the right-hand side of Eq. (28). An iteration on dP/dx is then performed until the value of dP/dx calculated is equal to the value chosen. When this process has converged, there is a mismatch between the two sides of Eq. (29), which is usually on the order of 2 to 3%.

Determination of the Mass Flow

Once conditions at the initial station are provided, the procedure described previously can be used to find the solution for a given mass flow, given Reynolds number, given nozzle geometry and wall-temperature distribution, and given gas properties. Usually, these solutions eventually display either of two types of behavior. In the first, the pressure reaches a minimum and dP/dx becomes positive after that. In the second, dP/dx becomes more and more negative, until a station is reached at which there is no solution that will match the left and right sides of either Eq. (28) or Eq. (29). These two types of behavior correspond to changes in sign of the numerator and denominator of Eq. (28). There is a range of Reynolds numbers and nozzle shapes for which a saddle point can be found, where the numerator and denominator change sign at the same point. For such cases, the only physically acceptable mass flow is the eigenvalue for which the solution passes through this saddle point.

The computer program described in Ref. 29 has the capability of determining this eigenvalue. An upper and lower bound for the mass flow are specified as input data, and a solution is calculated for a value of A halfway between these bounds. When this solution displays either of the types of behavior mentioned above, its value of the mass flow is used as a new upper or lower bound, and the process is repeated until the upper and lower bounds differ by some preassigned amount (usually four significant figures are specified). Once the mass flow has been determined in this way, a final solution is calculated. This integration is interrupted slightly upstream of the saddle point, and the pressure-gradient distribution is then chosen so as to force the solution to lie along a straight line through the saddle point, in the plane of the numerator and denominator of Eq. (28). As soon as this fitted portion of the solution passes through the saddle point, the iterative solution for dP/dx (satisfying the streamtube relation) is resumed.

IV. Initial Conditions

In order to start the calculation method described in the previous section, it is necessary to specify a value of P, and profiles of U and Θ, at some initial station. In applications of thin-boundary-layer theory to the present problem, this initial station is usually taken at the geometric throat of the nozzle; there the boundary layer is assumed to have zero thickness, and the pressure, velocity, and enthalpy are assumed equal to the values they would have in an isentropic, inviscid, one-dimensional channel flow.

In the present study, where results are sought at very low Reynolds numbers, this approximation is not acceptable; instead, the solution must be started far upstream of the throat. Asymptotic solutions of the slender-channel equations for slow flow in a converging cone were derived for this purpose. Analogous solutions of the Navier-Stokes equations for incompressible flow have been presented by Ackerberg.[30]

The initial solution was derived by expanding all of the dependent variables in inverse powers of the nozzle radius

$$U = \sum_{N=2} [U_N(\eta)/\sigma_W{}^N],\ W = \sum_{N=3} [W_N(\eta)/\sigma_W{}^N]$$

$$P = 1 + \sum_{N=3} (\pi_N/\sigma_W{}^N),\ \Theta = 1 + \sum_{N=4} [T_N(\eta)/\sigma_W{}^N] \tag{31}$$

These expansions are substituted into the equations of motion and boundary conditions, and coefficients of like powers of σ_W are equated. The resulting ordinary differential equations for $U_N(\eta)$ and $T_N(\eta)$ can be integrated explicitly. The solutions contain the coefficients π_N, which are related to the given mass flow by expanding Eq. (21)

$$A\left(1 - \frac{\pi_3}{\sigma_W{}^3} + \ldots\right) = \sigma_W{}^2 \int_0^1 \left(\frac{U_2}{\sigma_W{}^2} + \frac{U_3}{\sigma_W{}^3} + \ldots\right) \eta d\eta \tag{32}$$

The results for the first few terms are

$$U_2(\eta) = 4A(1 - \eta^2),\ T_4(\eta) = -16A^2Pr(1 - \eta^2)^2$$
$$\pi_3 = [32\gamma/3(\gamma - 1)]A/B \tan\theta \tag{33}$$

This result for $T_4(\eta)$ is valid for either thermal condition of the wall.

Simplified Initial Conditions

It is desirable to specify the initial conditions to a level of accuracy that is commensurate with the accuracy of the finite-difference scheme. From an inspection of Eq. (32), the indication is that mass conservation requires the U-profile to be specified through order $\sigma_W{}^{-5}$ and the pressure through order $\sigma_W{}^{-3}$. When this was done in an early version of the computer program, however, it was found that the higher-order contributions were masked by the truncation error in the finite-difference results—i.e., if dP/dx is specified through order $\sigma_W{}^{-3}$, a Simpson's rule integration of the resulting U profile at $x + \Delta x$ is in general different from the right side of Eq. (32) by an amount of order greater than $\sigma_W{}^{-5}$. For this reason, the iterative method of finding dP/dx was chosen. In this method, the value of dP/dx is adjusted until the values of the two sides of Eq. (29) are equal; this has the effect of doing numerically to dP/dx what the series coefficients π_N would do analytically. In this method, the series solution is used only to give the starting profiles, and an initial guess at dP/dx.

To be consistent with this procedure, the starting conditions were simplified to

$$U = U_2(\eta)/\sigma_W{}^2 + U_3(1)/\sigma_W{}^3 = 4A(1 - \eta^2)/\sigma_W{}^2 + 8AK_u/\sigma_W{}^3$$
$$\Theta = 1 + T_4(\eta)/\sigma_W{}^4,\ P = 1/(1 - \pi_3/\sigma_W{}^3)$$
$$dP/dx = -3\pi_3\sigma_W'/\sigma_W{}^4 \tag{34}$$

This approximate velocity profile fails to conserve mass at the initial station; the error introduced is typically less than 1%.

For all of the solutions presented in this paper, the initial station was chosen as $x_0 = -5$.

V. Results

In the subsections that follow, the nozzle geometry used is described first; following this, the general features of the flowfields found by changing various parameters are described. Results that relate specifically to performance characteristics (mass flow, thrust, specific impulse) are deferred to the end of this section.

Table 1 Summary of cases

Case no.	B	A	θ_1, deg	R_1	θ_2, deg	$(\Theta_W x)$	$x_{\text{point}}^{\text{saddle}}$
1	1250	0.1122	−20	13.356	21.77	adiabatic wall	4.95
2	1250	0.121	−20	0.5	22.4	adiabatic wall	1.05
3	1250	0.1222	−30	0.5	22.4	adiabatic wall	...
4	800	0.1188	−20	0.5	22.4	adiabatic wall	1.15
5	400	0.1138	−20	0.5	22.4	adiabatic wall	20
6	800	0.1188	−20	0.5	25.0	adiabatic wall	0.65
7	800	0.1188	−20	0.5	21.0	adiabatic wall	2.35
8	800	0.1188	−20	0.5	18.0	adiabatic wall	20
9	800	0.1188	−20	0.5	15.0	adiabatic wall	20
10	100	See text	−20	0.5	15.0	adiabatic wall	20
11	1250	0.1208	−20	0.5	22.4	$\Theta_W = 1.0$	1.45
12	1250	0.1370	−20	0.5	22.4	$1.0 \leq \Theta_W \leq 0.2$ (see text)	0.75

Geometry

The particular geometrical configuration used in the present study consisted of a convergent cone and a divergent cone, connected by a constant radius-of-curvature-section. The coordinates are given by

$$\sigma_W = x\tan\theta_1 + 1 + R_1(1 - \cos\theta_1 - \sin\theta_1\tan\theta_1), x \leq R_1\sin\theta_1$$

$$\sigma_W = 1 + R_1 - (R_1^2 - x^2)^{1/2}, \quad R_1\sin\theta_1 \leq x \leq R_1\sin\theta_2$$

$$\sigma_W = x\tan\theta_2 + 1 + R_1(1 - \cos\theta_2 - \sin\theta_2\tan\theta_2), x \geq R_1\sin\theta_2$$

Cases Studied

The computer program described earlier has been used to investigate the effects of varying some of the parameters of the problem. Table 1 lists the values used for the various parameters. For all cases, the values $\gamma = 1.4$, $Pr = 0.75$, $\omega = 0.9$, $\alpha_u = \alpha_T = 1.0$ were used. In general, a step size of $\Delta x = 0.1$ was used; however, for runs with the sharp throat ($R_1 = 0.5$), it was reduced to $\Delta x = 0.01$ in the region $-0.3 \leqslant x \leqslant +0.3$. All of the calculations reported here were done in double precision on an IBM 360/65, Release 14.

Comparison with Experiment

Case 1 provides a direct comparison with the experimental data reported by Yevseyev,[31] who carried out a very detailed probing of the low-density flow in a conical nozzle. Results for the centerline Mach number (taken from Yevseyev's Fig. 8) are presented in Fig. 1; the present calculation is 6% high at $x = 6$, and about 3% low at $x = 15$. A more stringent test of the calculation method is shown in Fig. 2 where the measured and calculated velocity profiles at $x = 11.1$ (see Yevseyev's Fig. 7) show excellent agreement.

It should be emphasized that the calculations shown contain no approximations beyond those implicit in the use of the slender-channel equations; they constitute the solution of the direct problem, for a specified nozzle geometry and a specified set of reservoir conditions. No attempt has been made to improve the agreement by varying the gas-property parameters.

Effects of Upstream Geometry

Cases 2 and 3 are identical except for the value of the inlet angle; the results of these two runs are indistinguishable for $x \geqslant 0$, and were taken as evidence that the upstream geometry has little effect on the flow. Obviously, much more evidence is needed before the quantitative limitations of this statement are clear, but it was felt that exploration of this effect could be deferred until after the variation of other parameters had been studied; all of the other cases described here used $\theta_1 = -20°$.

Effect of Reynolds Number

Cases 2, 4, and 5 show the effect of the Reynolds number. Before discussing this effect specifically, it is well to examine how the iteration process led to determination of the eigensolution. For case 2, Fig. 3 shows the variation of P with x at various values of the mass flow; these exhibit the two types of behavior described earlier. This behavior is shown more clearly in Fig. 4, which is the plane of the numerator and denominator of Eq. (28). After the iterations shown had been completed, the value $A = 0.121$ was selected as the eigenvalue of A, and this solution was interrupted at $x = 0$; it was then placed on a straight line through the saddle point, as shown in Fig. 4. The result of this fitting is shown in the P,x plane in Fig. 3. Note that the saddle point is crossed about one radius downstream of the throat; thereafter, the iterative method of finding dP/dx is resumed [using Eq. (28)], and continues to run stably.

An isometric view of the velocity and enthalpy profiles at various positions along the nozzle is shown in Fig. 5.

Lowering the Reynolds number B to 800 has the effect of moving the saddle point slightly farther downstream (case 4), and a further reduction to $B = 400$ moves it out beyond

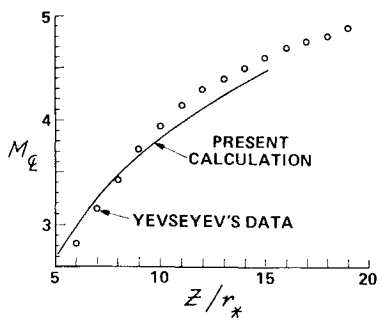

Fig. 1 Distribution of centerline Mach number, case 1.

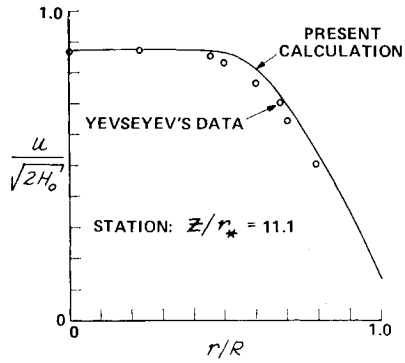

Fig. 2 Velocity—profile prediction, case 1.

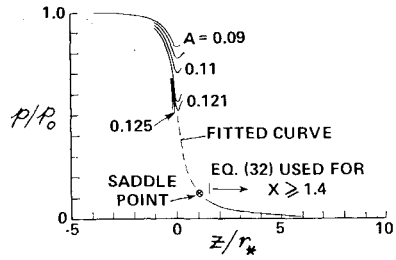

Fig. 3 Pressure distributions for various mass flows, case 2.

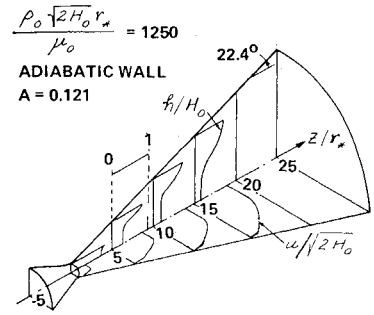

Fig. 5 Profiles of velocity and static enthalpy, case 2.

twenty radii (case 5). For this case, the solution in the plane of Fig. 4 moves along the straight-line segment toward the saddle point, but never reaches it.

Effect of Exit-Cone Angle

Cases 4 and 6–9 show the effect of changing the angle θ_2, at a constant Reynolds number $B = 800$. Reducing this angle inhibits the expansion to supersonic conditions, and so has the same effect as lowering B. As θ_2 becomes smaller, the saddle point moves farther down the nozzle, passing beyond twenty radii for $\theta_2 \lesssim 18°$. There is obviously a range of expansion angles and Reynolds numbers for which there is no unique supersonic solution of the problem determined by passage through the singular point.

Extended Study of the Nonsingular-Solution Region

The conditions of case 10 lie well within the region where there is no saddle point. A large number of computer runs was made for this case, and the resulting pressure distributions along the nozzle are shown in Fig. 6. At the lowest value of the mass flow ($A = 0.04$), dP/dx is negative out to forty radii; at somewhat higher mass flows, the pressure reaches a minimum, and then rises slightly as the flow continues to decelerate. Ultimately a pressure maximum is reached, and the final state of the flow is a Poiseuille velocity profile, with the static enthalpy uniformly equal to its wall value.

For sufficiently high mass flows, a choking condition is encountered; however, in contrast to the higher Reynolds number, higher θ_2 cases, the locus of zero pressure gradients does not intersect with the locus of infinite pressure gradients. The solution for $A = 0.08764252$ extends all the way to forty radii with dP/dx negative. Figure 6 shows this solution passing between the loci of the zero- and infinite-slope points.

For values of A greater than about 0.086, these solutions exhibit a zone of supersonic flow near the axis, and slightly downstream of the throat. Contours of constant Mach number are shown in Fig. 7 for the case $A = 0.08764252$. A smooth transition from supersonic back to subsonic conditions is predicted. This type of transition is possible within the framework of the slender-channel equations, where the axial gradients in the stress tensor (which could give rise to a shock-wave type of transition) have been neglected in comparison with transverse shear stresses. The Mach-number-distribution along these streamlines is analogous to that of a streamline entering the boundary layer on a flat plate in a supersonic flow; the Mach number decays below one as the streamline is carried deeper into the slower part of the boundary layer.

Figure 7 also shows the locus where the axial velocity reaches 99% of its centerline value. This locus shows how the boundary layer essentially closes on this flow. In all of these flows, the decreasing pressure generates two opposing effects: the first, appearing in the inviscid terms of the streamtube relation, is to accelerate the flow to a supersonic state. The opposing effect, appearing in the viscous terms, is to thicken the boundary layer. The conditions of case 10 lie in a region where the latter effect dominates the former; no acceleration to a permanent supersonic state is possible within the framework of the slender-channel equations, and the flow undergoes a transition back to subsonic conditions.

Whether a smooth transition of this type is realized experimentally is, to the author's knowledge, an open question. Measurements aimed at resolving this problem are needed; in addition, further analysis in which the longitudinal stress contributions are retained would be very useful.§

However, even if these predictions of an imbedded supersonic zone are accepted as having physical significance, there still remains a problem of predicting nozzle performance when the pressure imposed at the exit plane is extremely low. Figure 8 shows the slender-channel prediction of mass flow as a function of exit-plane pressure, if the nozzle is cut off at $x = 40$. The point to be noted is that no solutions were found for which p_e/p_0 was less than around 0.09. It seems probable that for values of A between 0.08764252 and 0.08764343, solutions could be found in which choking occurs arbitrarily far downstream. However, it may be that some mechanisms which are not included in the slender-channel equations must be invoked in order to predict how the flow adjusts to the exit conditions encountered in the space environment. In particular, the presence of a large subsonic region suggests that a strong upstream influence of the exit-plane conditions may be experienced in these flows.

Several authors (see, for example, Refs. 33 and 34) have reported experiments in which the exit-plane pressure appeared to have an anomalously large effect on the thrust level. It is possible that the observed phenomena are caused by the viscous suppression of supersonic conditions, in the manner revealed by the present solutions.

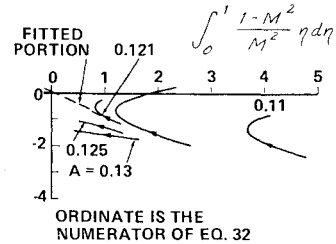

Fig. 4 Solution curves for various mass flows, case 2.

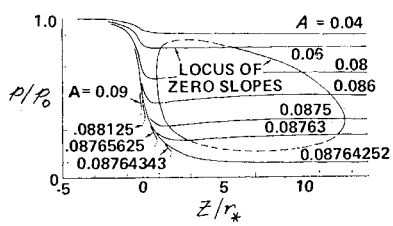

Fig. 6 Pressure distributions for various mass flows, case 10.

§ Sichel[32] has studied the limit opposite to the slender-channel case, in which transverse shear stresses are neglected compared to the longitudinal ones.

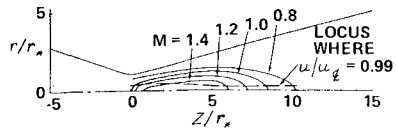

Fig. 7 Contours of constant Mach number, case 10, $A = 0.08764252$.

The precise boundary above which a unique supersonic solution can be found has not yet been adequately determined; the present results suggest that this will be the state of the flow if B is greater than 800 and θ_2 is greater than about 20°. This value of B corresponds to a throat Reynolds number around 300; using Sutherland and Maes' rule of thumb (see Ref. 1, p. 1160), this corresponds to a thrust level in the vicinity of 10^{-4} lbf for a typical nozzle size.

Effects of Heat Transfer and Variable Wall Temperature

Operation of a rocket device at low density implies that the thermal condition of the wall exerts a strong influence. Two cases were run in order to explore the effect of heat transfer on the flow. In the first of these (case 11) the wall temperature was equal to the reservoir temperature all along the nozzle. In the second, (case 12) the wall temperature was dropped from T_0 to $T_0/5$ between -4 and -2 radii, and was held constant thereafter:

$$\begin{aligned}\Theta_W &= 1.0, \quad -5 \leqslant x \leqslant -4\\ &= 0.6 + 0.4\cos[(x+4)\pi/2], \quad -4 \leqslant x \leqslant -2\\ &= 0.2, \quad x \geqslant -2\end{aligned}$$

This latter case was an attempt to simulate the thermal environment that might be encountered when the gas flows out of a hot reservoir and into a relatively cold channel. Cases 11 and 12 were the same as case 2 in all other respects.

The wall-temperature and heat-transfer distributions, and the variations of the total-enthalpy flux [which are related by Eq. (25)] are shown in Fig. 9, and typical profiles are given in Fig. 10. Profiles for the hot wall case are practically identical to those of the adiabatic-wall case, but the cold-wall case shows marked differences. In particular, in the cold-wall case, about 20% of the enthalpy flux is lost in heat transfer to the wall. Also, the discharge coefficient is greater than one—the nozzle can pass more mass flow than an isentropic, one-dimensional nozzle would, due to the elevated density level near the walls. The enthalpy profile in Fig. 10b has a slight bulge near the wall, typical of what happens in high Mach-number flows due to viscous heating.

A noticeable thinning of the boundary layer is also apparent with the cold wall. Figure 11 shows the variation of the displacement thickness with distance along the nozzle, compared to the constant-wall-temperature case. The displacement thickness used here is defined by

$$\int_0^R \rho u r dr = \rho_{\ell} u_{\ell} \int_0^{R-\delta_1} r dr$$

$$\frac{\delta_1}{r_*} = \sigma_W \left[1 - \left(2\int_0^1 \frac{DU}{(DU)_{\ell}}\eta d\eta\right)^{1/2}\right] \tag{35}$$

Conditions on the axis can be calculated with an error of a few

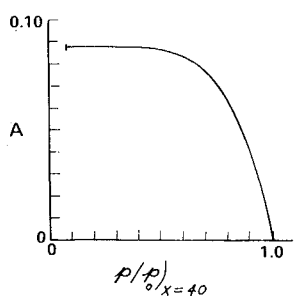

Fig. 8 Mass-flow variation with exit-plane pressure (exit station at $x = 40$), case 10.

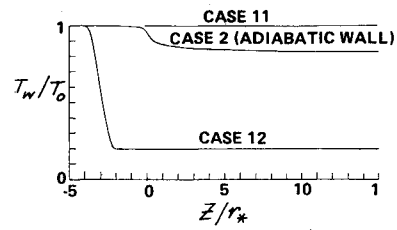

Fig. 9a Wall-temperature distributions.

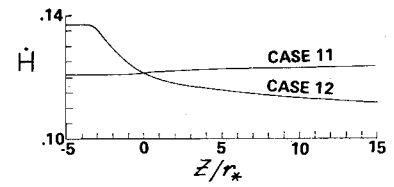

Fig. 9b Enthalpy-flux distributions.

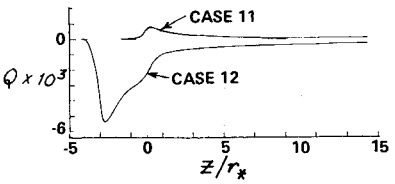

Fig. 9c Heat-transfer distributions.

percent, by using the isentropic, one-dimensional flow results at an effective area ratio found by subtracting the displacement thickness:

$$A_{\text{eff}}/A_* = (\sigma_W - \delta_1/r_*)^2$$

Thus the present results provide a corroboration, without a priori assumptions, that the displacement thickness is indeed the correct scale to use in making boundary-layer corrections to the core flow.

Performance Characteristics

The thrust coefficients obtained from these calculations are shown in Fig. 12, as a function of geometric area ratio. (No correction has been made for any effects that might accompany the transition from conditions at the given area ratio to zero-pressure ambient conditions.) For comparison, the ideal value at the same area ratio is shown. These were found from (see, Ref. 35, p. 446):

$$\bar{F} = \{[2\gamma^2/(\gamma-1)][2/(\gamma+1)]^{(\gamma+1)/(\gamma-1)} \times (1-P)^{(\gamma+1)/\gamma}\}^{1/2} + P\sigma_W^2$$

The effect of increasing Reynolds number is to increase the thrust coefficient, as might be expected (cases 2 and 4). Increasing θ_2 produced a slight increase in $\bar{F}$ (cases 4, 6, and 7), indicating that thrust losses due to divergence were not yet

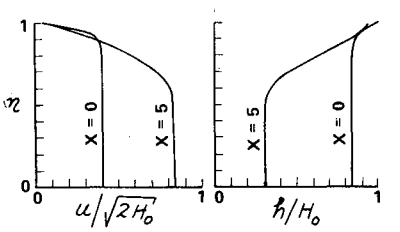

Fig. 10a Velocity and enthalpy profiles, case 11.

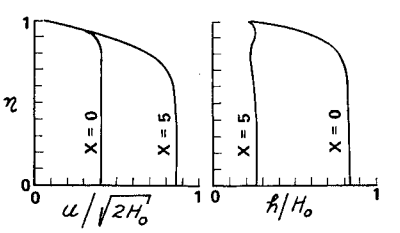

Fig. 10b Velocity and enthalpy profiles, case 12.

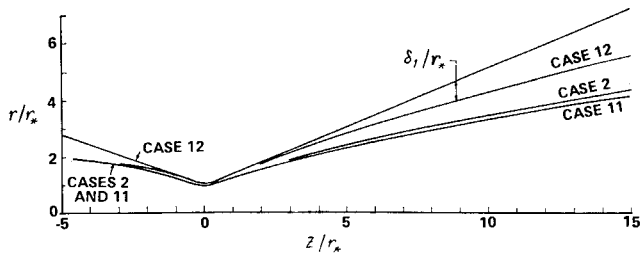

Fig. 11 Variation of displacement thickness.

dominant in the range shown here. Decreasing the longitudinal radius of curvature of the throat (cases 1 and 2) and cooling the wall (cases 12, 1, and 2) both increased the thrust markedly.

One interesting feature of the sharp-throat results is the rapid rise toward the maximum. For these configurations, the nozzle can be cut off at 5 radii with less than a five percent loss in thrust. These results illustrate the importance, in these calculations, of establishing the correct initial state of the flow at the throat.

In Fig. 12, the higher thrust coefficients are obtained at the expense of higher mass flows. The quantity $\bar{F}/A$, proportional to the specific impulse, is shown in Fig. 13. These results indicate that the specific impulse is a relatively weak function of Reynolds number and nozzle geometry, for the range investigated here. The strongest influence was that associated with strong cooling of the nozzle walls.

One indication for design practice is that performance is increased by using a sharp throat, and by cutting the nozzle off at a rather modest exit-area ratio. This indication must be used with some caution, however, until more extensive calculations and further comparisons with experiment are made.

VI. Concluding Remarks

The net result of the studies reported here is a computational method for finding a solution of the direct problem of low-density flow from given reservoir conditions through a nozzle of given shape. Results found by this method show good agreement with experiment. The equations used become identical with the thin-boundary-layer approximation at high Reynolds number, and can be used well down into the lower Reynolds number region where the importance of the state of the flow at the throat makes the conventional thin-boundary-layer model of limited value.

At the time of this writing, the number of cases that have been calculated is insufficient for any general conclusions regarding nozzle design. Within the limits of the calculations made, it appears that sharp throats lead to better performance, and that exit-area ratios as low as 10 can be employed without serious loss in specific impulse.

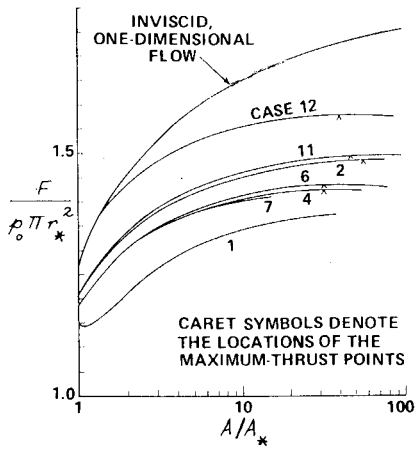

Fig. 12 Thrust-coefficient dependence on area ratio.

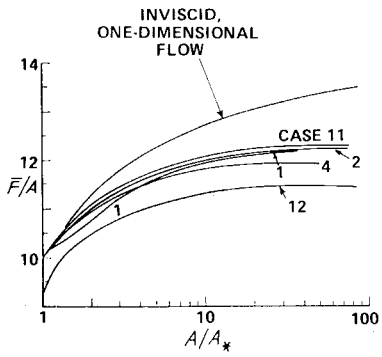

Fig. 13 Variation of specific-impulse parameter.

At sufficiently low Reynolds number and small divergence angles, the slender-channel equations do not have a solution in which the flow expands to supersonic conditions. Instead, the boundary layer completely fills the channel, and the solution takes on the character of a viscous, subsonic pipe flow. One implication of this result is that a relatively strong upstream effect of the exit-plane conditions is likely to be felt in these flows. Further clarification of this regime awaits experimental probing of the flow structure and the application of more complex analyses which retain some of the effects discarded in the slender-channel approximation.

References

[1] Sutherland, G. S. and Maes, M. E., "A Review of Micro-rocket Technology: 10^{-6} to 1 lbf Thrust," *Journal of Spacecraft and Rockets*, Vol. 3, No. 8, Aug. 1966, pp. 1153–1165.

[2] Murch, C. K. et al., "Low-Thrust Nozzle Performance," *Journal of Spacecraft and Rockets*, Vol. 5, No. 9, Sept. 1968, pp. 1090–1094.

[3] Spisz, E. W., Brinich, P. F., and Jack, J. R., "Thrust Coefficients of Low-Thrust Nozzles," TN D-3056, Oct. 1965, NASA.

[4] Luce, R. G., Gregorek, G. M., and Lee, J. D., "The Laminar Boundary Layer in Axisymmetric Hypersonic Nozzles with Wall Cooling," ARL-65-112, AD 620909, June 1965, Ohio State Univ., Columbus, Ohio.

[5] "Development of the Subliming Solid Control Rocket, Phase II," NASA CR-712, March 1967, Rocket Research Corp., Seattle, Wash.

[6] Durand, J. A. and Potter, J. L., "Calculation of Thickness of Laminar Boundary Layers in Axisymmetric Nozzles with Low-Density, Hypervelocity Flows," TN 61-146, Dec. 1961, Arnold Engineering Development Center, Tullahoma, Tenn.

[7] Rasmussen, M. L. and Karamcheti, K., "Viscous Effects Far Downstream in a Slowly Expanding Hypersonic Nozzle," *AIAA Journal*, Vol. 4, No. 5, May 1966, pp. 807–815.

[8] Williams, J. C., "A Study of Compressible and Incompressible Viscous Flow in Slender Channels," Rept. 83-213, June 1962, Univ. of Southern California, Los Angeles, Calif.

[9] Williams, J. C., "Viscous Compressible and Incompressible Flow in Slender Channels," *AIAA Journal*, Vol. 1, No. 1, Jan. 1963, pp. 186–195.

[10] Pan, Y. S. and Probstein, R. F., "Rarefied Flow Transition at a Leading Edge," *Fundamental Phenomena in Hypersonic Flow*, edited by J. G. Hall, Cornell University Press, Ithaca, N.Y., 1965, pp. 259–306.

[11] Zeiberg, S. L. and Bleich, G. D., "Finite-Difference Calculation of Hypersonic Wakes," *AIAA Journal*, Vol. 2, No. 8, Aug. 1964, pp. 1396–1402.

[12] Langan, W. T., Cresswell, J. D., and Browne, W. G., "Effects of Ablation Products on Ionization in Hypersonic Wakes," *AIAA Journal*, Vol. 3, No. 12, Dec. 1965, pp. 2211–2218.

[13] Chen, T. and Wen, K. S., "FORTRAN Computer Code for the Axisymmetric Viscous Wake Analysis of a Hypersonic Reentry Body," AC DRL TR 66-66, 1966, General Motors Corp., Santa Barbara, Calif.

[14] Baum, E. and Denison, M. R., "Interacting Supersonic Laminar Wake Calculations by a Finite Difference Method," *AIAA Journal*, Vol. 5, No. 7, July 1967, pp. 1224–1230.

[15] Greco, R. V. and Stoner, W. A., "Research and Development of a 1-kw Plasmajet Thruster," *AIAA Journal*, Vol. 1, No. 2, Feb. 1963, pp. 320–324.

[16] "Equations, Tables, and Charts for Compressible Flow," Rept. 1135, 1953, NACA.

[17] Weinbaum, S. and Garvine, R. W., "On the Two-Dimensional Viscous Counterpart of the One-Dimensional Sonic Throat," *Journal of Fluid Mechanics*, Vol. 39, 1969, pp. 57–85.

[18] Garvine, R. W. and Weinbaum, S., "The Axially Symmetric Throat Phenomenon in Interacting Viscous-Inviscid Flows," *Proceedings of the 1969 Symposium on Viscous Interaction Phenomena in Supersonic and Hypersonic Flow*, University of Dayton Press, Dayton, Ohio, 1970, pp. 427–461.

[19] Shapiro, A. H., *The Dynamics and Thermodynamics of Compressible Fluid Flow*, Vol. 1, Ronald Press, New York, 1953, Chap. 8.

[20] Lighthill, M. J., "On Boundary Layers and Upstream Influence, II. Supersonic Flows without Separation," *Proceedings of the Royal Society (London), Ser. A*, Vol. 217, 1953, pp. 478–507.

[21] Williams, J. C., "Conical Nozzle Flow with Velocity Slip and Temperature Jump," *AIAA Journal*, Vol. 5, No. 12, Dec. 1967, pp. 2128–2134.

[22] Williams, J. C., "Conical Nozzle Flow of Viscous Compressible Gas with Energy Extraction," *Applied Scientific Research*, Vol. 19, 1968, pp. 285–301.

[23] Adams, J. C., "Similar Solutions for Viscous Compressible Laminar Flow in Slender Axisymmetric Channels," Ph.D. thesis, 1966, North Carolina State Univ.

[24] Flugge-Lotz, I. and Baxter, D. C., "The Solution of Compressible Laminar Boundary-Layer Problems by a Finite-Difference Method," Pt. I, TR-103, Sept. 1956; Pt. II, TR-110, Oct. 1957, Stanford Univ., Stanford, California.

[25] Wu, J. C., "The Solution of Laminar Boundary-Layer Equations by the Finite-Difference Method," *Proceedings of the 1961 Heat Transfer and Fluid Mechanics Institute*, Stanford University Press, Stanford, Calif., 1961, pp. 55–69.

[26] Milligan, M. W., "Low Density Gas Flow through Varying Area Passages," Ph.D. thesis, 1963, Univ. of Tennessee.

[27] Myers, W. A., "A Numerical Solution of Viscous Compressible Flow in Slender Channels," M.S. thesis, June 1964, N65-14576, AD 605441, Univ. of Tennessee.

[28] Richtmeyer, R. D. and Morton, K. W., *Difference Method for Initial-Value Problems*, 2nd ed., Interscience, New York, 1967, pp. 275–282.

[29] Rae, W. J., "Final Report on a Study of Low-Density Nozzle Flows with Application to Microthrust Rockets," Rept. AI-2590-A-1, Dec. 1969, Cornell Aeronautical Lab., Buffalo, N.Y.

[30] Ackerberg, R. C., "The Viscous Incompressible Flow Inside a Cone," *Journal of Fluid Mechanics*, Vol. 21, 1965, pp. 47–81.

[31] Yevseyev, G. A., "Experimental Investigation of Flow of Rarefied Gas," *Akademiia Nauk, SSSR, Izvestiia, Mekhanika*, No. 3, 1965, pp. 165–172; translation MT-67-22, March 31, 1967, U.S. Air Force Systems Command, Foreign Technology Div., Wright-Patterson Air Force Base, Ohio.

[32] Sichel, M., "The Effect of Longitudinal Viscosity on the Flow at a Nozzle Throat," *Journal of Fluid Mechanics*, Vol. 25, 1966, pp. 769–786.

[33] Kanning, G., "Measured Performance of Water-Vapor Jets for Space Vehicle Attitude Control Systems," TN D-3561, Aug. 1966, NASA.

[34] John, R. R., "Final Report: Resistojet Research and Development, Phase II," NASA CR-54688, Dec. 1966, Avco Research and Technology Lab., Wilmington, Mass.

[35] Summerfield, M., "The Liquid Propellant Rocket Engine," *Jet Propulsion Engines*, edited by O. E. Lancaster, Princeton University Press, Princeton, N.J., 1959, Sec. G.